sustainability

MDPI

Article

Dual-Purpose Utilization of Sri Lankan Apatite for Rare Earth Recovery Integrated into Sustainable Nitrophosphate Fertilizer Manufacturing

D. B. Hashini Indrachapa Bandara, Avantha Prasad, K. D. Anushka Dulanjana and Pradeep Wishwanath Samarasekere *

Center for Advanced Materials and Smart Manufacturing, Faculty of Computing and Technology, University of Kelaniya, Kelaniya 11600, Sri Lanka
* Correspondence: pradeeps@kln.ac.lk

Abstract

Rare earth elements (REEs) have garnered significant global attention due to their essential role in advanced technologies. Sri Lanka is endowed with various REE-bearing minerals, including the apatite-rich deposit in the Eppawala area, commonly known as Eppawala rock phosphate (ERP). However, direct extraction of REEs from ERP is technically challenging and economically unfeasible. This study introduces a novel, integrated approach for recovering REEs from ERP as a by-product of nitrophosphate fertilizer production. The process involves nitric acid-based acidolysis of apatite, optimized at 10 M nitric acid for 2 h at 70 °C with a pulp density of 2.4 mL/g. During cooling crystallization, 42 wt% of calcium was removed as $Ca(NO_3)_2.4H_2O$ while REEs remained in the solution. REEs were then selectively precipitated as REE phosphates via pH-controlled addition of ammonium hydroxide, minimizing the co-precipitation with calcium. Further separation was achieved through selective dissolution in a sulfuric–phosphoric acid mixture, followed by precipitation as sodium rare earth double sulfates. The process achieved over 90% total REE recovery with extraction efficiencies in the order of Pr > Nd > Ce > Gd > Sm > Y > Dy. Samples were characterized for their phase composition, elemental content, and morphology. The fertilizer results confirmed the successful production of a nutrient-rich nitrophosphate (NP) with 18.2% nitrogen and 13.9% phosphorus (as P_2O_5) with a low moisture content (0.6%) and minimal free acid (0.1%), indicating strong agronomic value and storage stability. This study represents one of the pioneering efforts to valorize Sri Lanka's apatite through a novel, dual-purpose, and circular approach, recovering REEs while simultaneously producing high-quality fertilizer.

Keywords: Eppawala rock phosphate; apatite; rare earth elements; REE recovery; fertilizer production; nitrophosphate; green mining; mineral valorization

Academic Editor: Piotr Celary

Received: 27 April 2025
Revised: 15 June 2025
Accepted: 20 June 2025
Published: 11 July 2025

Citation: Bandara, D.B.H.I.; Prasad, A.; Dulanjana, K.D.A.; Samarasekere, P.W. Dual-Purpose Utilization of Sri Lankan Apatite for Rare Earth Recovery Integrated into Sustainable Nitrophosphate Fertilizer Manufacturing. *Sustainability* **2025**, *17*, 6353. https://doi.org/10.3390/su17146353

1. Introduction

Rare earth elements (REEs) comprise a group of seventeen metals, including the fifteen lanthanides (from lanthanum (La) to lutetium (Lu)), along with yttrium (Y) and scandium (Sc). Due to their similar electronic configurations, lanthanides often exhibit comparable chemical and physical properties [1]. The REEs are typically categorized into two subgroups: light rare earth elements (LREEs), ranging from lanthanum to samarium, and heavy rare earth elements (HREEs), which include the remaining lanthanides along with yttrium.

The extraction and recovery of REEs have gained global attention due to their critical role in diverse high-technology applications [2]. REEs are often referred to as "the vitamins of modern industry" because of their contributions to improving energy efficiency, miniaturization, speed, durability, and thermal stability in various advance technologies [3]. Although they are lithophiles in nature and are relatively abundant in the Earth's crust, REEs are rarely concentrated in economically viable mineral deposits. Their extraction is complicated by the geochemical similarity among REEs and between REE gangue minerals, making the identification and processing of concentrated deposits particularly complex and resource-intensive.

China currently dominates the global REE supply chain, but other countries such as Australia, the United States, Brazil, China, Russia, India, and Vietnam also possess REE-bearing mineral resources with varying concentrations [3,4]. REEs are typically found in minerals such as bastnaesite [(Ce, La)(CO_3)F], xenotime (YPO_4), monazite [(Ce, La, Nd)(Th)PO_4)], loparite [(Ce, Na, Ca)(Ti, Nb)O_3], apatite [(Ca, REE, Sr, Na, K)$_3$$Ca_2$(PO4)$_3$(F, OH)], and ion-adsorption clays [4–9]. Among these, bastnaesite and monazite are the most commercially exploited sources.

Apatite, a group of phosphate minerals, is primarily used for producing phosphate fertilizers and phosphoric acid [10–13]. Its general formula is $Ca_{10}(PO_4)_6(X_2)$, where X can be OH^-, F^-, or Cl^-, giving the compounds hydroxyapatite ($Ca_{10}(PO_4)_6(OH)_2$), fluorapatite ($Ca_{10}(PO_4)_6$ F_2), and chlorapatite ($Ca_{10}(PO_4)_6$ Cl_2) [14]. Apatite can incorporate REEs through iconic substitution for Ca^{2+} and P^{5+} within its crystal lattice, typically containing 0.1–0.8% REE oxides [15]. Although this concentration is relatively low, increasing global demand for REEs has led to renewed interest in apatite as an alternative source of REEs.

The Sri Lankan geological setting is favorable for REE mineralization, with known occurrences in Pulmoddai beach placer deposits [16], Eppawala carbonatite [17], alluvial placer deposits [18], gem deposits [5] and granitic rock deposits [7]. Among these, the Eppawala apatite deposit, located in the North Central province, is the country's first known carbonatite occurrence and contains elevated concentrations of La (510–577 ppm), Ce (1217–1714 ppm), and Nd (637–856 ppm) [17]. Despite its potential, REE extraction from Eppawala rock phosphate has been minimally explored due to the uneconomical nature of direct extraction using conventional methods [17–19].

Phosphate is a non-renewable, essential nutrient for plant growth, with phosphate rock being almost exclusively used in the production of phosphate fertilizers such as single superphosphate (SSP), triple superphosphate (TSP), and nitrophosphate [11,20–22]. These are typically produced using sulfuric, phosphoric, and nitric acid, respectively. However, the SSP and TSP production processes are associated with the formation of phosphogypsum, a waste by-product that retains up to 85% of the REEs, complicating recovery and creating economic and environmental concerns.

In contrast, the nitrophosphate fertilizer production route offers a more favorable pathway for REE recovery. In this process, apatite is digested with nitric acid, and REEs can be selectively recovered from the nitrophosphoric solution through a partial neutralization process, precipitating as REE phosphates. Previous studies suggest this route allows for more efficient REE extraction compared to the SSP or TSP processes. Furthermore, nitrophosphate fertilizers are valued for their balanced nutrient profiles, typically containing plant-available forms, such as ammonium nitrate (NH_4NO_3), monoammonium phosphate ($NH_4H_2PO_4$), and dicalcium phosphate ($CaHPO_4$).

This study presents a novel dual-purpose strategy that integrates REE recovery with the production of nitrophosphate fertilizer using apatite from the Eppawala deposit. By leveraging a resource traditionally used solely for phosphorus, this integrated process enables the simultaneous extraction of valuable REEs and essential agricultural nutrients,

aligning with circular economy principles and enhancing resource efficiency. Impotently this work represents the first reported attempt to valorize Sri Lanka's 60-million-ton rock phosphate deposit, through sustainable REE recovery, offering a pathway towards greater economic value addition and enhanced resource utilization efficiency.

2. Materials and Methods

2.1. Materials

The phosphate concentrate used in this study was obtained from an apatite deposit located near the Eppawala area in the North Central province of Sri Lanka. Powdered Eppawala rock phosphate samples were obtained from the mining site through Lanka Phosphate Ltd.in Eppawala, Sri Lanka. ERP samples were first dried at 80 °C for 24 h, ground, and homogenized to a fine powder. The ground powder was mechanically sieved by a sieve shaker (MRC Laboratory equipment TSS-200, Holon, Israel), and the sieved portion with a particle size less than mesh No. 230 (62 μm) was separated as the fine fraction to achieve a more uniform particle size distribution.

The following analytical-grade (AR) reagents were used: nitric acid (HNO_3, 65 wt%, VWR Chemicals, Mississauga, ON, Canada), ammonium hydroxide (NH_4OH, 25 wt%, VWR Chemicals, Mississauga, ON, Canada), anhydrous ethanol (C_2H_5OH, 99 wt%, Sigma Aldrich, Bengaluru, India), sodium chloride (NaCl, 99.9%, SRL Chemicals, Mumbai, India), and sodium sulfate (Na_2SO_4, >99 wt%, HiMedia Laboratories, Thane, India). Ethylene glycol of industrial grade was obtained. Distilled water was used in all experimental procedures.

2.2. Characterization

The mineralogical composition of Eppawala rock phosphate (ERP) was characterized using X-ray diffraction (XRD) on a Rigaku Ultima IV diffractometer (Rigaku, Akishima, Japan), operated at 30 mA and 40 kV with Cu Kα radiation (λ = 1.5406 Å), 1.20 KW power, and a 2θ scan range of 5° to 90° with a step size of 0.02°. Phase identification was performed using Profex (2015, Version 5.4.1) software based on Rietveld refinement [23]. Elemental compositions were analyzed in triplicate by Inductively Coupled Plasma Optical Emission Spectrometry (ICP-OES, Agilent 5800, Agilent Technologies, Bayan Lepas, Malaysia) to quantify REEs and other elements in the samples, ensuring analytical accuracy through multi-point calibration and internal standards. The phosphate concentration in leachate was determined calorimetrically via the phosphovanadomolybdate method using UV-Vis spectrophotometry. Morphological and microstructural features were analyzed using a Scanning Electron Microscope (SEM) integrated with Energy-Dispersive X-ray Spectroscopy (EDX) on a Hitachi Su6600 FE-SEM (Field Emission Scanning Electron Microscope, Hitachi High-Technologies Inc., Tokyo, Japan) and an Oxford instruments EDX (Oxford Instruments NanoAnalysis, High Wycombe, UK) with AZtec software (Version 6.1). SEM images were obtained using a secondary electron (SE) detector, and the instrument was calibrated using a cobalt standard. Samples were coated with gold prior to imaging. EDX analysis was conducted at an accelerating voltage of 15 kV, for reliable detection and mapping of the elemental composition on the mineral surfaces. Fertilizer quality testing of synthesized nitrophosphate fertilizer was conducted at the Industrial Technology Institute (ITI), Sri Lanka.

All ICP-OES and UV-Vis measurements were performed in triplicate (n = 3), and the results are presented as averages. Calibration was performed using standard multi-element solutions, and instrument calibration was validated using internal standards and certified reference materials where available.

2.3. Methods

The REE recovery process, integrated with nitrophosphate fertilizer production, was carried out in six major steps: acid digestion (acidolysis) of ERP; cooling crystallization for calcium removal; partial neutralization to precipitate REE phosphates; selective dissolution of REEs; precipitation of sodium REE double sulfates; final recovery, separation, and purification of REEs.

2.3.1. Acidolysis of Rock Phosphate

Acidolysis was performed using 25 g of ERP and varying to acid-to-solid weight ratios (1 mL/g to 3 mL/g) of nitric acid (5 M to 12 M), at temperatures ranging from 40 °C to 90 °C, for durations between 30 min and 180 min. Reactions were performed in a reactor fitted with a vertical water-cooled reflux condenser to limit nitric acid loss through volatilization, continuously stirring at 400 rpm. The overall acidolysis reaction is given in Equation (1).

$$Ca_5(PO_4)_3F_{\,(S)} + 10HNO_{3\,(aq)} \rightarrow 5Ca(NO_3)_{2\,(aq)} + 3H_3PO_{4\,(aq)} + HF_{\,(q)} \quad (1)$$

The leachate was filtered through a 0.2 µm membrane under vacuum, and both the residue and filtrate were analyzed. The leaching efficiency of REEs (x) was calculated using Equation (2).

$$x = \frac{R2}{R1} \times 100\% \quad (2)$$

where $R1$ is the REE content in the raw ERP and $R2$ is the REE content in the leachate.

The phosphate decomposition efficiency of P_2O_5 (α) was calculated using Equation (3).

$$\alpha = \frac{P2}{P1} \times 100\% \quad (3)$$

where $P1$ is the P_2O_5 content in raw ERP and $P2$ is the P_2O_5 content in leachate.

The digestion efficiency of ERP (DE) was determined by using Equation (4).

$$DE = \frac{W2}{W1} \times 100\% \quad (4)$$

where $W1$ is the initial weight of ERP and $W2$ is the dissolved weight of ERP after the acid digestion process.

2.3.2. Cooling Crystallization

To reduce calcium interference, the leachate was cooled in a chiller bath at −5 °C to −20 °C for 90 min to precipitate calcium nitrate tetrahydrate ($Ca(NO_3)_2.4H_2O$), which was then filtered. The co-precipitation efficiency of REEs (σ) was calculated using Equation (5).

$$\sigma = \left(1 - \frac{R3}{R2}\right) \times 100\% \quad (5)$$

where $R3$ is the REEs in the mother liquor after the cooling crystallization, and $R2$ is the REEs in the initial leachate.

The calcium removal efficiency (μ_1) from the remaining mother liquor was calculated using Equation (6).

$$\mu_1 = \left(1 - \frac{C2}{C1}\right) \times 100\% \quad (6)$$

where $C1$ is the CaO in the original leachate and $C2$ is in the mother liquor after the cooling crystallization.

2.3.3. Partial Neutralization

The mother liquor was partially neutralized using 25% NH_4OH at 70 °C under stirring. The pH of the solution was adjusted to 1.4 to selectively precipitate REEs. The precipitate was centrifuged, washed with ethanol, and dried at 80 °C for 24 h and characterized via XRD and ICP-OES. The filtrate consisting of the nitrophosphate acid solution was analyzed to determine any residual REEs. The extraction efficiency of the REEs (β) was determined by Equation (7).

$$\beta = \left(1 - \frac{R4}{R3}\right) \times 100\% \quad (7)$$

where $R4$ is the REEs remaining in the filtrate after partial neutralization.

2.3.4. Nitrophosphate Fertilizer Synthesis

The remaining filtrate (nitrophosphate acid solution) was fully neutralized to produce nitrophosphate fertilizer. Standard fertilizer quality parameters such as moisture content, total phosphate, water-soluble phosphate, free phosphoric acid, and total nitrogen were measured following fertilizer guidelines.

2.3.5. Selective Dissolution of REE

The precipitate from the partial neutralization containing REE phosphates and residual calcium and iron was treated with a mixture of 36% phosphoric acid and 15% sulfuric acid at room temperature to selectively dissolve REEs, leaving Ca as insoluble $CaSO_4$. The dried $CaSO_4$ was weighed, and the calcium ion removal efficiency (μ_2) was determined by Equation (8).

$$\mu_2 = \frac{C3}{C1 - C2} \times 100\% \quad (8)$$

where $C3$ is the CaO content in the $CaSO_4$.

The REE dissolution efficiency (γ) was calculated using Equation (9).

$$\gamma = 1 - \frac{R5}{R3 - R4} \times 100\% \quad (9)$$

where $R5$ is the REEs remaining in $CaSO_4$.

2.3.6. Sodium Rare Earth Double Sulfate Precipitation

REEs in the phosphoric–sulfuric acid solution were precipitated as sodium double sulfates by adding NaCl or Na_2SO_4, at 80 °C:

$$Na^{+}{}_{(aq)} + REE^{3+}{}_{(aq)} + 2SO_4^{2-}{}_{(aq)} + XH_2O_{(l)} \rightarrow Na\,REE(SO_4)_2 \cdot XH_2O_{(s)} \quad (10)$$

The precipitate was filtered, washed with deionized (DI) water, dried at 80 °C, and dissolved in nitric acid for ICP-OES analysis. The final REE recovery efficiency (ε) was calculated using Equation (11).

$$\varepsilon = \frac{R7}{R6} \times 100\% \quad (11)$$

where $R6$ is the REEs in the phosphoric–sulfuric acid solution and $R7$ is the REEs in the double sulfate precipitate.

3. Results

3.1. Chemical Characterization of Eppawala Rock Phosphate

The elemental composition of Eppawala rock phosphate (ERP) was determined via ICP-OES.

As shown in Table 1, ERP contains 25.88% P_2O_5, confirming its high phosphate content. Major constituents include CaO and SiO_2 with minor amounts of Fe_2O_3, Al_2O_3, Na_2O, and other trace elements. The total concentration of rare earth elements (REEs) was measured at 2465.3 mg/kg, with Ce being the dominant component (1124.9 mg/kg, 45.63%), followed by La (482.7 mg/kg) and Nd (477.7 mg/kg) (Table 2).

Table 1. Major elemental composition of Eppawala rock phosphate (ERP).

Component	SiO_2	Al_2O_3	BaO	CaO	Fe_2O_3	K_2O	MgO	MnO	Na_2O	P_2O_5
(*w*/*w*) %	15.29	5.64	0.21	39.51	6.80	0.24	0.54	0.25	1.32	25.88

Table 2. Rare earth element composition of Eppawala rock phosphate (ERP).

Rare Earth Elements	Ce	Dy	Gd	La	Nd	Pr	Sm	Y
ppm (mg/kg)	1124.9	1.5	41.4	482.7	477.7	138.1	72.3	90.0

3.2. Effect of Nitric Acid Concentration on Leaching

A series of optimization experiments were conducted to determine the optimum nitric acid concentration for maximizing both ERP digestion and REE recovery. The experiments were performed at 70 °C, for 120 min, with a pulp density of 2.4 mL/g. In Figure 1, it is shown that the ERP digestion efficiency improved from 68.3% to 82.8% and P_2O_5 decomposition increased from 44.6% to 99.6% as the acid concentration increased from 5 M to 10 M. However, beyond 10 M, both the digestion and decomposition efficiencies declined, indicating reduced acidolysis performance (see Table S1. Digestion efficiency and P_2O_5 decomposition at different nitric acid concentrations in acid leaching of ERP).

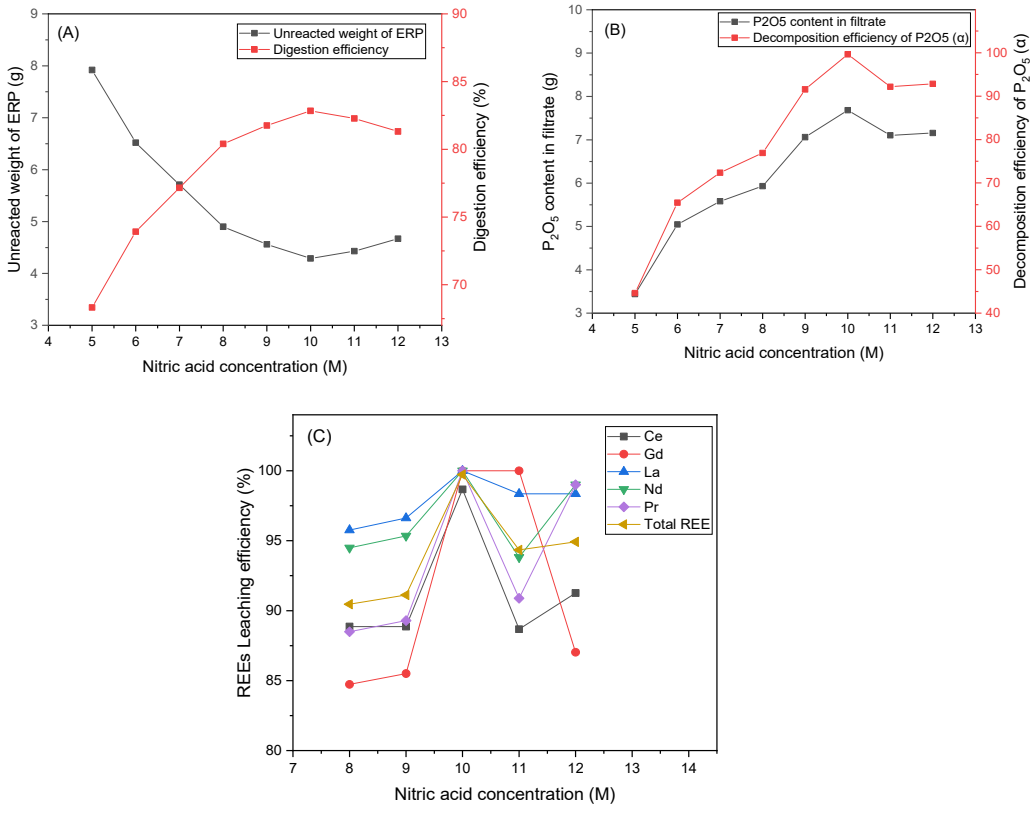

Figure 1. Leaching performance as a function of nitric acid concentration: (**A**) Aaid concentration vs. digestion efficiency and unreacted ERP weight; (**B**) acid concentration vs. P_2O_5 content and decomposition efficiency; (**C**) acid concentration vs. leaching efficiency of REEs.

In Figure 1C, it is shown that REE leaching efficiency increased from 90.5% to 99.7% between 8 M and 10 M, but dropped to 94.9% at 12 M. The increase in solution viscosity of nitric acid at higher concentrations likely hindered the P_2O_5 decomposition and REE diffusion from the phosphate to the acid solution. Therefore, 10 M nitric acid was identified as the optimal concentration for acidolysis (see Table S2. REE leaching efficiency % with different nitric acid concentrations in acid leaching of ERP).

3.3. Effect of Leaching Temperature

The effect of temperature on ERP digestion and REE leaching was studied from 40 °C to 90 °C. In Figure 2, it is shown that digestion efficiency increased from 69.4% to 85.3%, and P_2O_5 decomposition increased from 83.0% to 92.6% up to 80 °C. A decline in both efficiencies was observed beyond this point, with digestion reducing to 78.4% and decomposition to 81.6% at 90 °C. In Figure 2C, it is shown that REE leaching efficiency peaked at 99.7% at 70 °C and remained high (99.0%) at 80 °C, but declined to 93.4% at 90 °C. Thus, 70 °C was selected as the optimal temperature for subsequent experiments (see Table S3. Digestion efficiency and P_2O_5 decomposition at different leaching temperatures in acid leaching of ERP and Table S4. REE leaching efficiency % with different acidolysis temperatures in acid leaching of ERP).

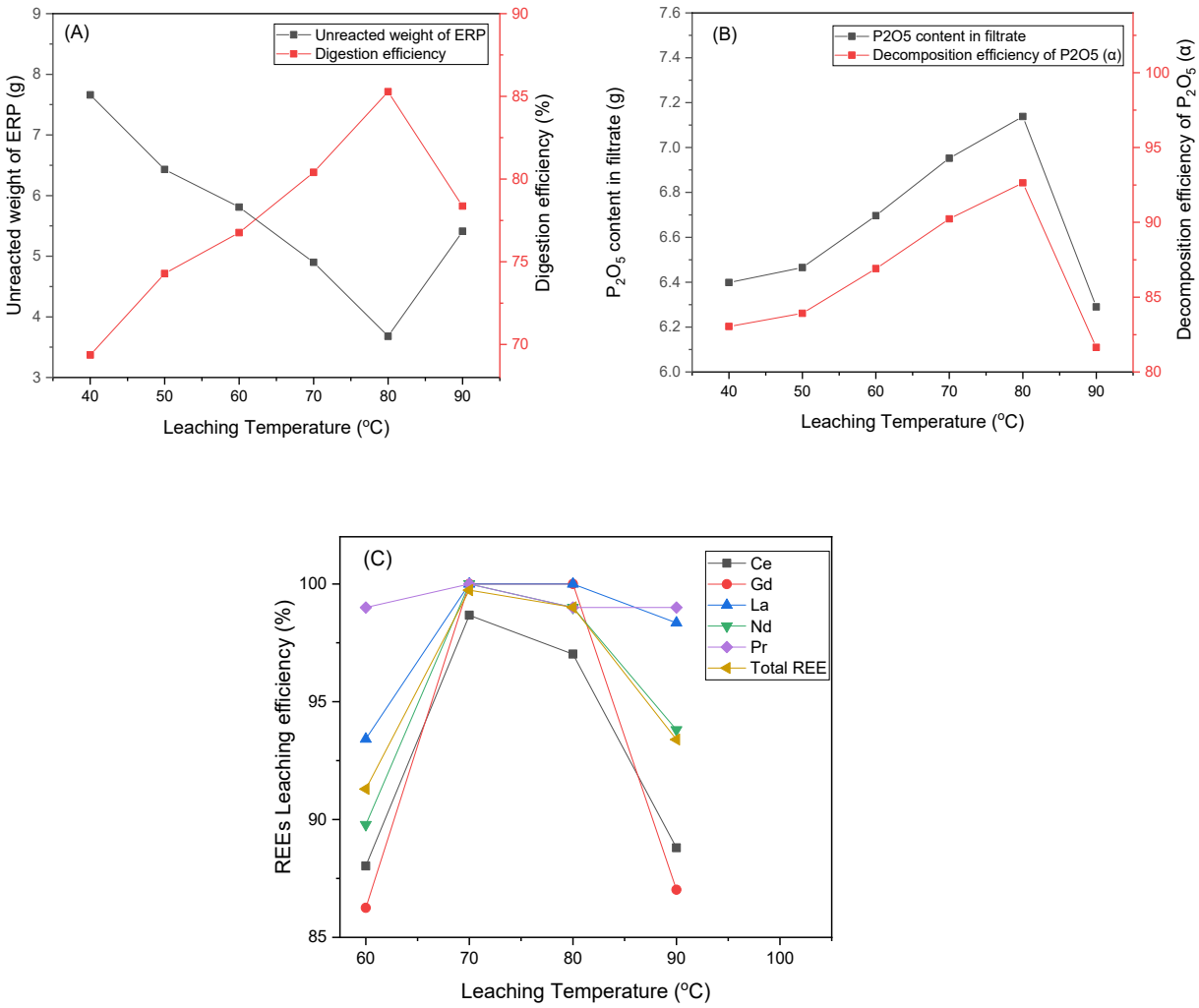

Figure 2. Effect of leaching temperature on ERP decomposition: (**A**) Temperature vs. unreacted ERP weight and digestion efficiency; (**B**) Temperature vs. P_2O_5 content and decomposition efficiency; (**C**) Temperature vs. REE leaching efficiency.

3.4. Effect of Leaching Time

In Figure 3, it is indicated that digestion and P_2O_5 decomposition efficiencies increased with leaching time from 30 to 120 min. The digestion efficiency increased from 76.8% to 85.3%, and the decomposition efficiency increased from 59.7% to 92.6%. Beyond 120 min, a reduction was noted, likely due to re-precipitation or degradation. REE leaching efficiency also peaked at 99.7% at 120 min and slightly declined to 98.6% at 180 min. Based on this, a leaching time of 120 min was determined as optimal (see Table S5. Digestion efficiency and P_2O_5 decomposition at different leaching times in acid leaching of ERP and Table S6. REE leaching efficiency % with different acidolysis times in acid leaching of ERP).

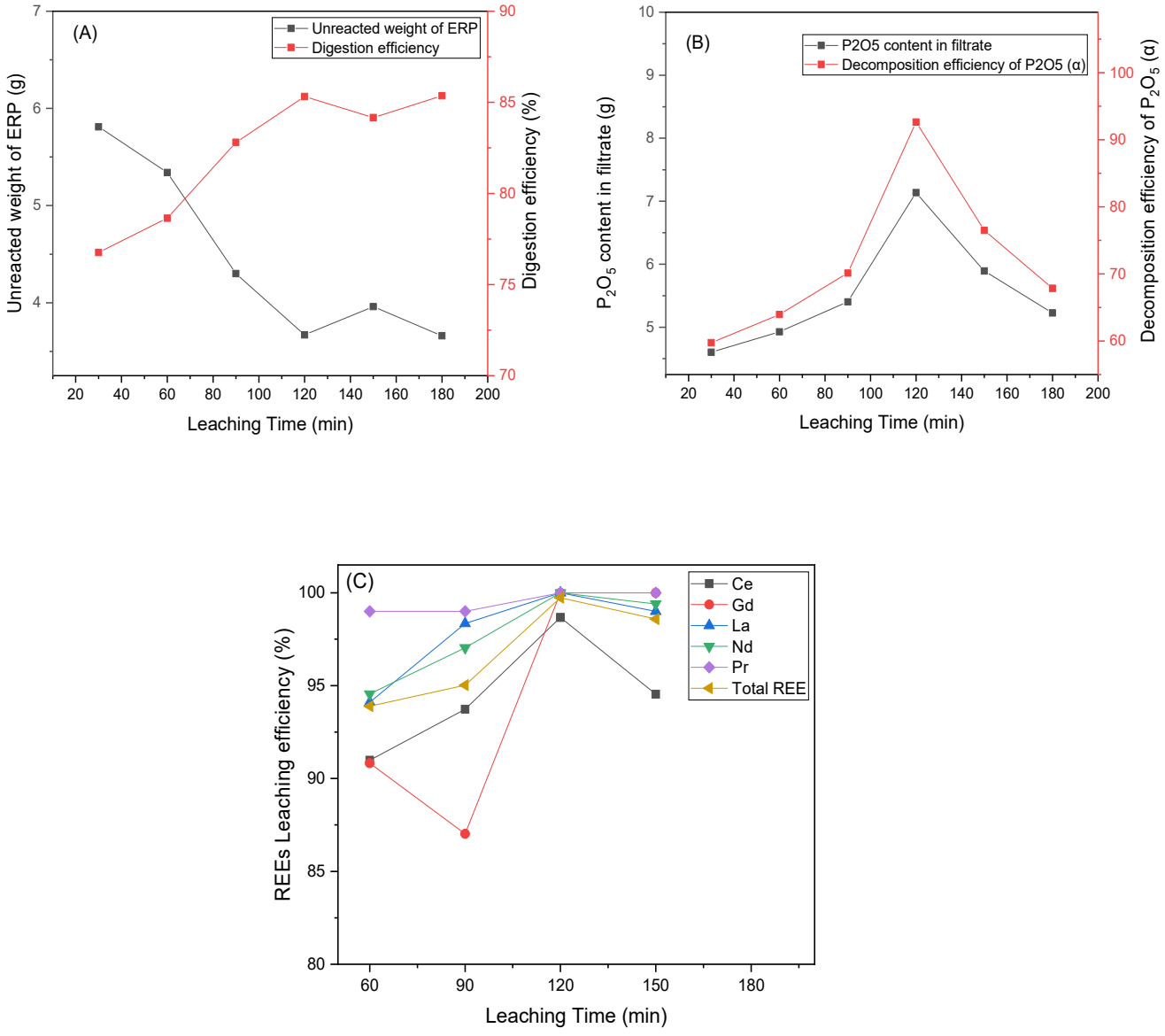

Figure 3. Effect of leaching time on ERP decomposition and REE recovery: (**A**) time vs. unreacted ERP weight and digestion efficiency; (**B**) time vs. P_2O_5 content and decomposition efficiency; (**C**) time vs. REE leaching efficiency.

3.5. Effect of Pulp Density

In Figure 4 it is presented that increasing the pulp density from 1 to 3 mL/g enhanced ERP digestion and P_2O_5 decomposition. Digestion efficiency reached a maximum of 88.4% at 3 mL/g, while decomposition peaked at 80.0%. REE leaching improved from 91.3% at 2.0 mL/g to a maximum of 99.7% at 2.4 mL/g. No significant gains were observed at

3 mL/g (99.1%), confirming 2.4 mL/g as the optimal pulp density for REE recovery (see Table S7. Digestion efficiency and P_2O_5 decomposition at different leaching times in acid leaching of ERP and Table S8. REE leaching efficiency % with different pulp densities in acid leaching of ERP).

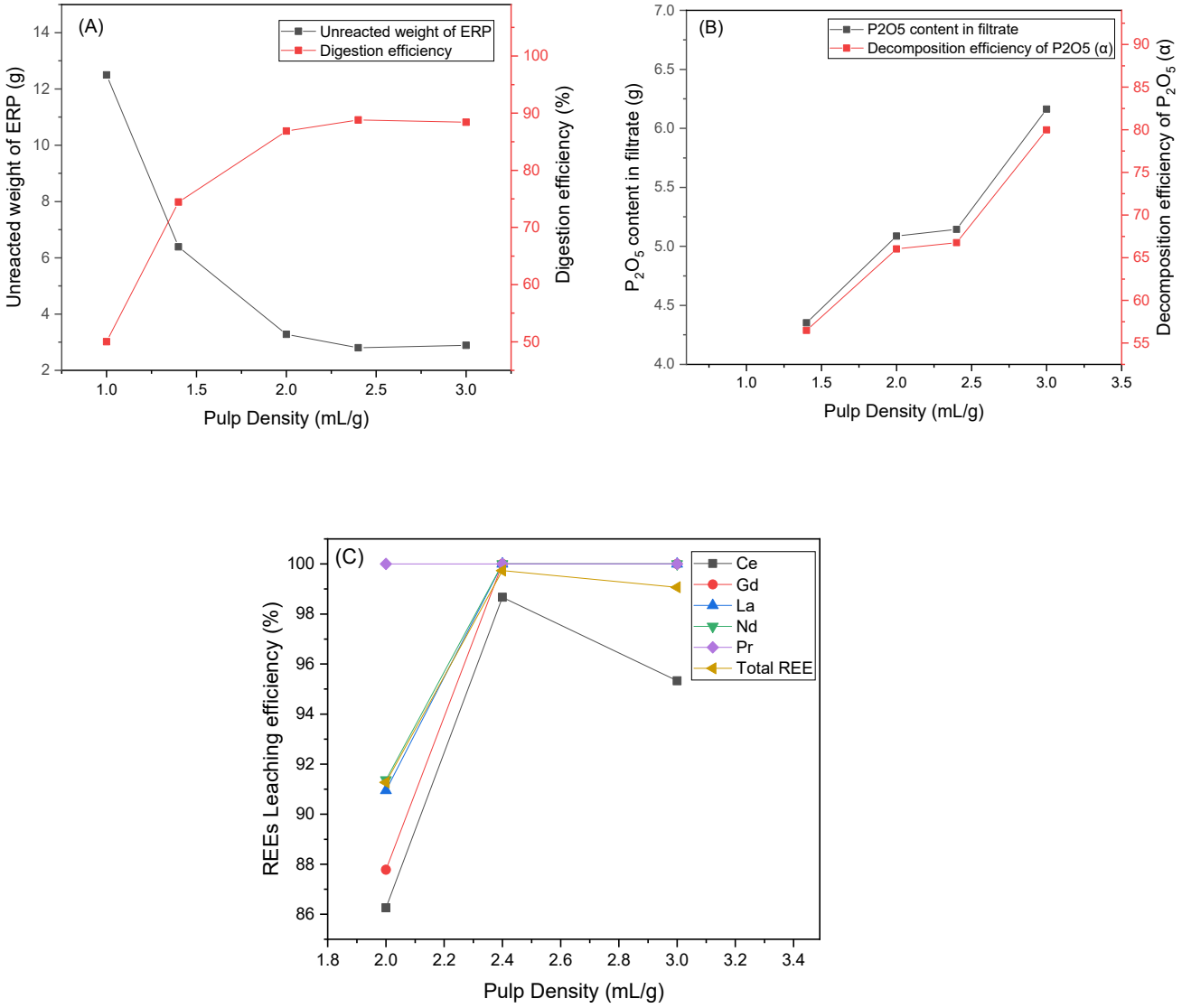

Figure 4. Effect of pulp density on ERP digestion and REE recovery: (**A**) pulp density vs. unreacted ERP weight and digestion efficiency; (**B**) pulp density vs. P_2O_5 content and decomposition efficiency; (**C**) pulp density vs. REE leaching efficiency.

Based on the optimized parameters of 10 M nitric acid, 2.4 mL/g pulp density, 120 min leaching time, and 70 °C leaching temperature, 25 g of ERP was acid-leached. The resulting filtrate was analyzed for its elemental composition, with REE leaching efficiency results summarized in Table 3.

Table 3. Leaching efficiency of REEs from ERP under optimized conditions and the degree of REE co-precipitation with $Ca(NO_3)_2 \cdot 4H_2O$.

REE	Ce	Gd	Dy	La	Nd	Pr	Sm	Y
Leaching Efficiency (%)	95.4	89.3	99.9	98.1	100	92.3	100	100
Co-precipitation (σ) %	1.6	1.6	1.8	0.5	1.8	0.5	1.2	2.0

3.6. Selective Recovery of REEs

Following acid leaching, the filtrate was subjected to a cooling crystallization, at −5 to −20 °C, achieving 42.0% calcium removal efficiency (μ_1). Calcium was precipitated as $Ca(NO_3)_2 \cdot 4H_2O$, with minimal REE co-precipitation (<2%) (Figure S1). According to the results summarized in Table 3, it is indicated that the degree of REE co-precipitation with $Ca(NO_3)_2 \cdot 4H_2O$ (σ) is relatively low. REEs were then selectively precipitated via partial neutralization using 25% NH_4OH, forming $REPO_4$ (Figure S2). ICP-OES analysis of the solution post-precipitation showed >90% REE recovery, as summarized in Table 4.

Table 4. REE extraction efficiency (β) % and selective dissolution efficiency (γ) %.

REE	Ce	Dy	Gd	La	Nd	Pr	Sm	Y
Extraction efficiency %	98.8	92.5	98.5	95.8	99.5	100	98.2	97.9
Selective dissolution efficiency %	99.8	99.9	99.9	99.8	99.8	99.9	100.0	99.9

Selective dissolution with a phosphoric–sulfuric acid mixture enabled the efficient separation of REEs from calcium. Calcium precipitated as insoluble calcium sulfate ($CaSO_4$) (Figure S3), while REEs remained in the solution, achieving 99% REE dissolution efficiency and confirming negligible REE incorporation in $CaSO_4$ (Table 4).

REEs were finally precipitated as a white polycrystalline powder of sodium rare earth double sulfate ($NaREE(SO_4)_2 \cdot xH_2O$) upon the addition of a sodium salt to the solution (Figure S4). Elemental analysis of the precipitated showed 22.2% REEs as the total REEs (TREEs) with sodium as the major component (68.4%), followed by Ca (4.9%), Fe (2.2%), and Al (2.17%). The results are summarized in Table 5, and it is shown that there are varied REE recovery efficiencies (ε), with Dy (59.5%) and Pr (52.5%) having the highest recoveries, while Gd had the lowest recovery (19.6%). These differences in efficiency are attributed to the ionic radius, solubility, and stability of their respective double sulfate complexes.

Table 5. Weight percentage of elements in ($NaREE(SO_4)_2 \cdot xH_2O$) %.

Elements	Na	Ca	Fe	Al	Mn	Mg	REEs
%	68.4	4.9	2.2	2.2	<0.1	<0.1	22.2
REE recovery efficiency (ε) from ($NaREE(SO_4)_2 \cdot xH_2O$) as a percentage of TREEs							
REE	**Ce**	**Dy**	**Gd**	**La**	**Nd**	**Pr**	**Sm**
TREE %	31.2	59.5	19.6	24.9	34.9	52.5	29.6

3.7. Nitrophosphate Synthesis

Following the separation of REEs, the residual filtrate, enriched in nitrate and phosphate from the partial neutralization step was converted into a value-added nitrophosphate fertilizer through a subsequent neutralization process. The nitrophosphoric solution was further neutralized with ammonium hydroxide at 80–90 °C. The resulting precipitate was centrifuged and oven-dried at 110 °C for 24 h. The final dried product was characterized physiochemically to evaluate its suitability as a nitrophosphate fertilizer (Table 6).

The final fertilizer exhibited a low moisture content of 0.6%, indicating superior physical stability and low hygroscopicity. Such low moisture levels are advantageous for field handling and storage of the fertilizer product, reducing the risk of caking and maintaining granular integrity. The total nitrogen content was 18.2%, a notably high value for nitrophosphate fertilizers, reflecting the efficient incorporation of nitrate species into

the final product. This indicates that nitric acid not only serves as a solubilizing agent for phosphate minerals but also contributes significantly to nitrogen enrichment, resulting in a dual-nutrient fertilizer with enhanced suitability for nitrogen-demanding crops. The total phosphorus content was measured as 13.9% as P_2O_5, demonstrating the successful solubilization of phosphorus from ERP. This phosphorus content is within the range of typical nitrophosphate or nitrogen–phosphorus–potassium (N-P-K) fertilizers and indicates the potential for the use of this fertilizer for field-level phosphorus delivery. The free phosphoric acid content was limited to 0.1% by mass, suggesting efficient neutralization, minimizing environmental risks, improving agronomic safety, and reducing the risk of soil acidification. These results confirm the successful production of a dual-nutrient fertilizer with strong agronomic and economic potential.

Table 6. Results of fertilizer testing.

Parameter	Results (% by Mass)	Method
Moisture	0.60	SLS 645 Part 2: 2023 [24]
Total nitrogen content as N, present by dry basis	18.20	AOAC 892.01 [25] SLS 645 Part 1: 2023 [26]
Total phosphate content as P_2O_5, percent by dry basis	13.90	SLS 645 Part 5: 1985 [27]
Free phosphoric acid as P_2O_5, percent by dry basis	0.10	SLS 812: 2014: Appendix B [28]

3.8. Evolution of Crystalline Phases and Surface Composition

The phase and crystal structure of the Eppawala rock phosphate before and after treatment for the recovery of REE phosphate were analyzed using X-ray diffraction (XRD), as shown in Figure 5. The XRD pattern of untreated ERP indicated a mixture of crystalline phases and the primary mineral phases of apatite and quartz [29]. The apatite phase contained crystalline phases of chlorapatite ($Ca_5(PO_4)_3Cl$) [30], hydroxyapatite ($Ca_5(PO_4)_3OH$) [31], and fluorapatite ($Ca_5(PO_4)_3F$) [32]. The diffraction peak at $2\theta = 25.8°$, with a corresponding d-spacing of 3.45 Å, is indicative of fluorapatite, while the peak at $2\theta = 31.5°$ (d = 2.836 Å) aligns with chlorapatite. The diffraction peak appearing at $2\theta = 36.5°$, with a corresponding d-spacing of 2.458 Å, is consistent with apatite. Considering the mineralogical diversity reported in the Eppawala deposit, it is likely that this reflection arises from a combination of these closely related phases [33]. The XRD pattern of the acid-treated ERP indicated the enrichment of REEs in the solid phase, with co-precipitation of $REPO_4$ and $Ca_3(PO_4)_2$ phases (Figure 5B). It was further noticed that the characteristic peaks of chlorapatite and fluorapatite disappeared in the treated sample, indicating the removal of anionic impurities, particularly Cl^- and F^- ions, during the leaching process [30,32]. Additionally, iron was also enriched in the treated solids as iron phosphate ($FePO_4 \cdot 2H_2O$) and iron hydrogenophosphates ($FeH_2P_2O_7$) [34,35], which were later effectively removed by cooling crystallization and the selective recovery of REEs as sodium rare earth double sulfates, as confirmed by the chemical analysis of the final precipitate.

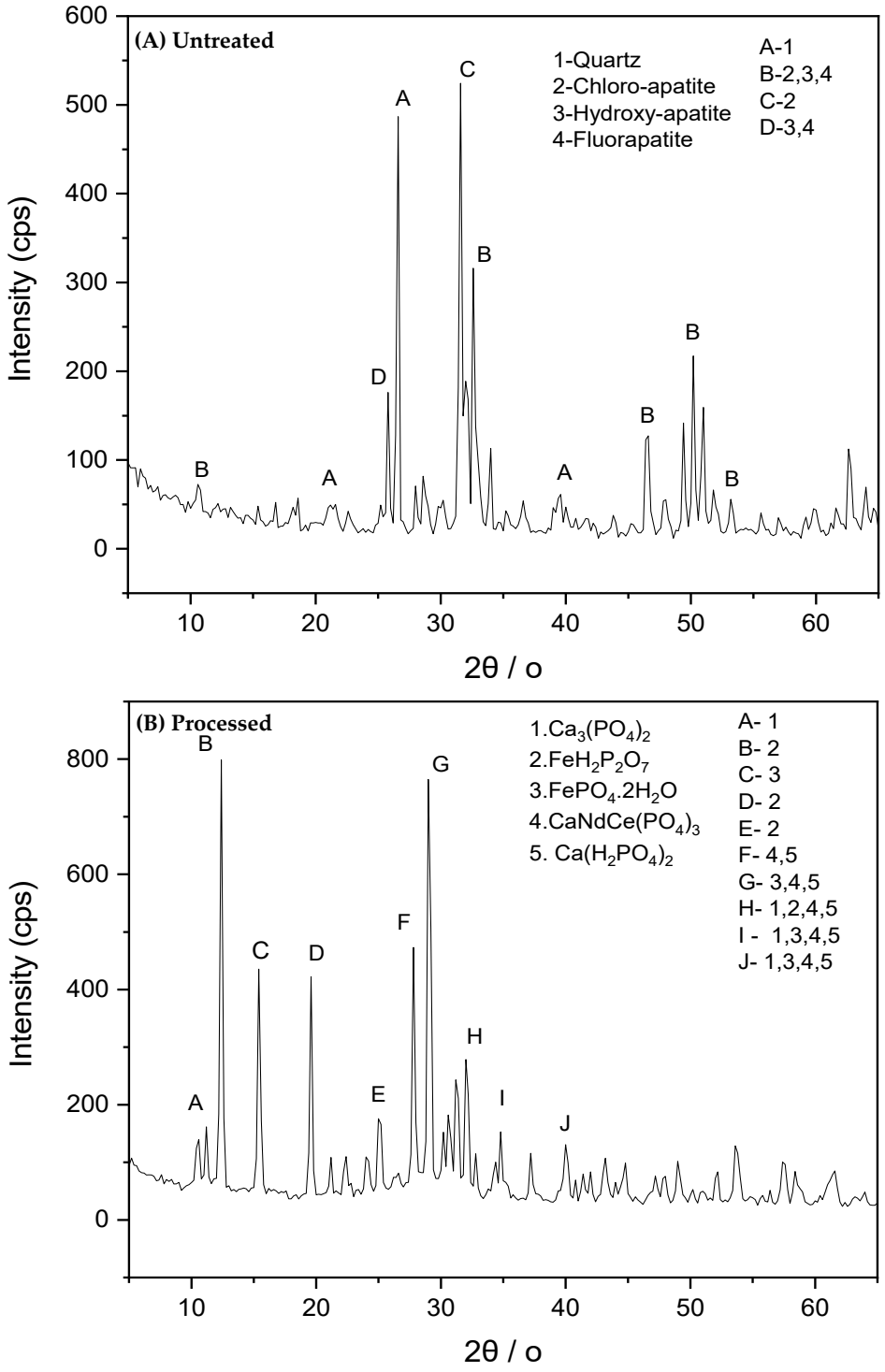

Figure 5. XRD analysis of ERP samples: (**A**) raw Eppawala rock phosphate (ERP) showing chlorapatite, hydroxyapatite, and fluorapatite phases; (**B**) treated ERP after acid leaching, showing $REPO_4$ and $Ca_3(PO_4)_2$ co-precipitation.

The morphological transformations of Eppawala rock phosphate were examined using Scanning Electron Microscopy coupled with Energy-Dispersive X-ray Spectroscopy (SEM-EDX), (Figure 6). The SEM micrograph of the untreated sample (Figure 6A) revealed predominantly irregular particles, generally smaller than 100 μm, with some fine particles adhering to the surfaces. The corresponding EDX mapping (Figure 6B) confirmed that the raw rock phosphate primarily contained Ca, Fe, Al, Si, P, Cl, and O prior to any chemical

treatment. The raw apatite samples exist as coarse, heterogeneous microstructures characterized by irregular, angular grains with distinct grain boundaries. This observation suggests the presence of a diverse range of minerals beyond apatite, with silica and quartz likely being among the dominant secondary phases. Following acid leaching and partial neutralization, significant morphological and phase changes were observed. In Figure 6C, it is shown that new crystalline phases began to form, with the surface appearing noticeably more crystalline and uniform compared to the raw ERP. The treated sample exhibited a mix of small spherical crystals and elongated prismatic structures, with particle sizes estimated at around 10 µm. This textural refinement suggests the successful formation of new phosphate phases through controlled pH precipitation. These distinct features disappeared upon conversion to nitrophosphate, which showed a more weathered and transformed morphology. The surface of the raw rock phosphate was characterized by a dense and compact texture with minimal porosity. In contrast, the nitrophosphate product exhibited a largely non-crystalline appearance with increased porosity and the presence of irregular, asymmetrical voids. The particles were arranged in loosely clustered and asymmetrical structures, were distributed non-uniformly (monodispersed), and showed substantial surface deformation (Figure 6D). These morphological changes provided visual confirmation of the successful solubilization of apatite into soluble phosphate forms during the nitrophosphate formation process. Figure 7 presents the EDX elemental mapping of the synthesized nitrophosphate fertilizer, highlighting Ca, P, N, and O as the predominant elements present in the final product. Importantly, no detectable levels of REEs were observed in the mapping. Although the map was acquired under limited dwell time and moderate resolution conditions, it qualitatively illustrates that the REEs were successfully separated during the preceding processing stages, confirming their effectiveness in producing a nutrient-rich fertilizer product.

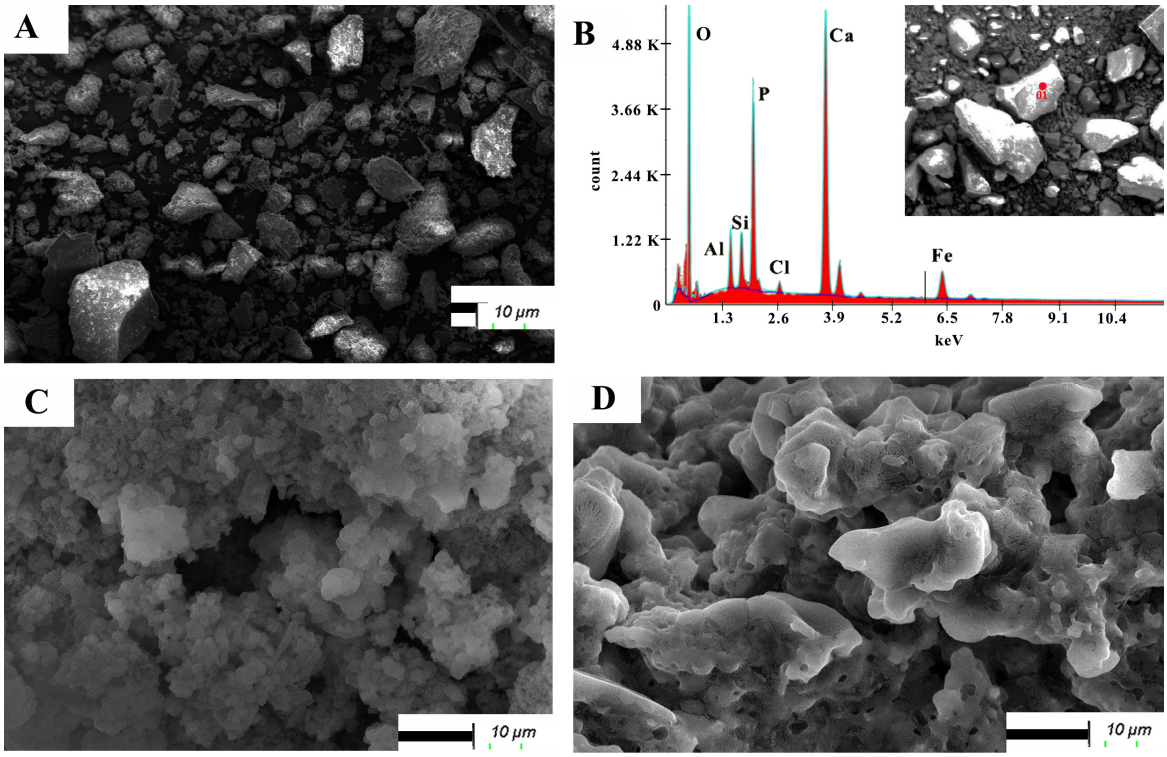

Figure 6. SEM-EDX characterization of ERP and nitrophosphate: (**A**) SEM image and (**B**) EDX spectrum of raw ERP; (**C**) SEM image showing morphological changes and new phase formation after leaching and partial neutralization; (**D**) SEM images of the synthesized nitrophosphate, highlighting a non-crystalline, porous structure.

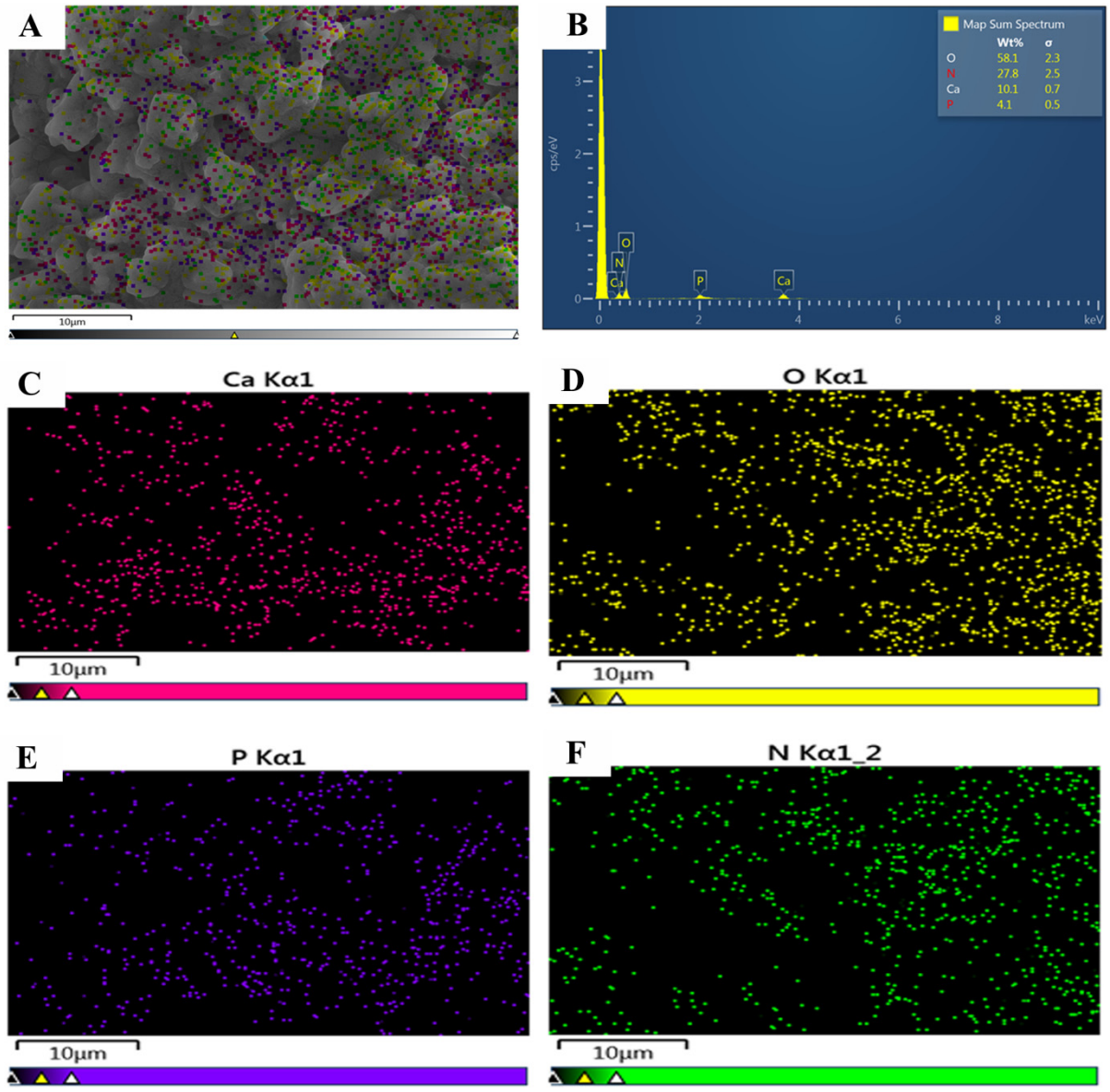

Figure 7. (**A**) EDX elemental mapping with the, (**B**) EDX spectrum of the synthesized nitrophosphate fertilizer showing (**C**) calcium, (**D**) oxygen, (**E**) phosphorus, and (**F**) nitrogen as the major detected elements. No signals corresponding to REEs were detected, supporting their effective separation during processing. Note: The map is intended as a qualitative representation.

4. Discussion

The chemical characterization of ERP confirms its potential for dual-purpose utilization, serving both as a phosphate-rich feedstock for fertilizer production and as a secondary source of REEs. The high P_2O_5 content (25.88%) supports its suitability for agrochemical applications, while the measurable concentration of total REE content (2465.3 mg/kg) indicates a viable opportunity for REE recovery, adding further strategic opportunity for value-added recovery from the mineral resource.

Based on the elemental composition data, the total concentration of LREEs (comprising Ce, La, Nd, Pr, and Sm) in ERP is 2295.7 mg/kg, while the total concentration of HREEs (including Gd, Dy, and Y) is 132.9 mg/kg. This yields an LREE/HREE ratio of 17.3, indicating a substantial predominance of LREEs in the deposit. In the apatite structure, Ca^{2+} can be partially substituted by REE ions. LREEs, with their larger ionic radii, closely match the size of Ca^{2+}, facilitating a more stable and energetically favorable substitution.

Conversely, HREEs have smaller ionic radii, making them less compatible with the calcium sites in the apatite lattice, leading to their reduced incorporation [36]. In comparison, the apatite concentrate studied in a Swedish apatite deposit contained a higher total REE content of 4516 mg/kg. This is approximately twice the total REE content in ERP and corresponds to an LREE/HREE ratio of approximately 2.74 [37]. Moreover, the apatite concentrate from Sweden contains a significantly higher proportion of HREEs compared to the Eppwala rock phosphate deposit in Sri Lanka, indicating a greater potential for the recovery of critical HREEs from the Swedish material.

The CaO/P_2O_5 ratio in the ERP sample is approximately 1.53 (39.51% CaO/25.88% P_2O_5). In the context of industrial fertilizer manufacturing, particularly the wet process for phosphoric acid production, the CaO/P_2O_5 ratio plays a pivotal role. A ratio exceeding 1.6 is generally considered uneconomical due to increased acid consumption during processing. The ERP's ratio of 1.53 falls just below this threshold, suggesting that it is marginally suitable for wet-process applications without incurring excessive acid use [38]. The CaO/P_2O_5 ratio of Mongolian apatite stands at approximately 1.78, derived from its chemical composition of 32.75% CaO and 18.30% P_2O_5. This ratio substantially exceeds the commonly accepted industrial threshold of 1.6 for phosphate rocks intended for wet-process applications [39].

Optimizing the leaching process is essential to efficiently extract both phosphates and REEs from ERP. The optimized acid leaching conditions obtained in this study, 10 M HNO_3, 70 °C, 120 min, 2.4 mL/g pulp density, significantly improved both phosphate solubilization and REE extraction, achieving REE leaching efficiencies above 99% in some cases. These results align with previous studies demonstrating the strong leachability of REEs from apatite-type ores under high acid concentrations, particularly in nitric acid media [40].

Apatite is a stable form of the natural phosphate, while the solid forms of rare earth phosphates are also stable, as indicated by their large equilibrium constants (pK_{sp} $CePO_4$ ~ 26.2) in comparison to complex species in solutions (log β $Ce(H_2PO_4)^{2+}$ ~ 1.92 and $Ce(HPO_4)^{+}$ ~ 4.32) [41]. Studies have demonstrated that higher concentrations of strong acids, such as nitric acid, improve the dissolution of REEs from apatite-based ores. It is well-established that REE phosphates are soluble in strong acids [42–46]. Consequently, increasing the concentration of nitric acid enhances the leaching efficiency of REEs from apatite minerals. In optimized acid leaching conditions using nitric acid, the extraction efficiency of REEs from phosphate minerals typically follows the order yttrium (Y) > lanthanum (La) > cerium (Ce). This sequence aligns with the solubility products (Ksp) of their respective phosphate compounds, where REE phosphates with higher Ksp values are more soluble and thus more readily leached [47]. Also, rare earth nitrate compounds formed in the acid leaching step are more soluble in nitrophosphoric media. This is because there was significant leaching efficiency of REE in the leachate (more than 90%), as proven by the elementary composition data given by ICP-OES after the acid leaching step (Table 3).

During the cooling crystallization step (−20 °C to −5 °C), calcium was selectively precipitated from the leachate as $Ca(NO_3)_2{\cdot}4H_2O$, despite the solution containing various other dissolved species such as iron (Fe^{3+}/Fe^{2+}), and REE^{3+}. A small amount of REE also co-precipitated with $Ca(NO_3)_2{\cdot}4H_2O$, yet this was limited to less than 2%. This minor co-precipitate may be due to the similarity in ionic radii between Ca^{2+} ions and REE^{3+} [36]. The overall efficiency of calcium removal in this process was approximately 42% by mass, indicating a partial removal of calcium ions under these conditions. This partial removal aligns with the known solubility behavior of calcium nitrate tetrahydrate under these cooling conditions [48]. $Ca(NO_3)_2{\cdot}4H_2O$ exhibits a solubility of 144 g per 100 g H_2O at 25 °C, whereas the rare earth nitrates have a higher solubility at the same temperature; for

example, cerium nitrate hexahydrate ($Ce(NO_3)_3 \cdot 6H_2O$) has a higher solubility of 176 g per 100 g H_2O at the same temperature [49]. This significant difference in solubility ensures that REE nitrates such as cerium nitrate remain in the aqueous phase, minimizing their co-precipitation with calcium compounds. The solubility of calcium nitrate increases due to its hygroscopic nature when the temperature is increased and correspondingly decreases upon cooling [48,50]. This leads to its crystallization in a stable tetrahydrate form. This precipitated calcium nitrate can be repurposed as a nitrogen-rich fertilizer, particularly when blended with urea [48]. Thus, each stage of the rare earth element extraction process using the nitrophosphate route not only facilitates efficient separation but also enhances overall value by producing agriculturally beneficial by-products. The resulting leachate upon the removal of cooling crystallization primarily consists of REE^{3+}, Fe^{3+}/Fe^{2+}, NO_3^-, and PO_4^{3-} ions and remaining Ca^{2+} ions. This leachate was then subjected to partial neutralization using 25% NH_4OH, adjusting the pH to approximately 1.4. The hydrogen ion concentration (pH value) significantly influences the solubility of REEs, as shown with phosphoric acid systems [44]. At lower pH levels, that is, at higher H^+ concentrations, REEs tend to remain soluble due to the increased protonation of phosphate species, which reduces their availability to form insoluble REE–phosphate complexes. Conversely, as the pH increases, that is, at lower H^+ concentrations, the deprotonation of phosphate species is facilitated, leading to a greater presence of hydrogen phosphate (HPO_4^{2-}) and phosphate (PO_4^{3-}) ions that facilitate REE precipitation through complexation and subsequent solid formation. The presence of phosphate ions induces the precipitation of REEs, enhancing their ability to bind with REEs and form precipitates. This behavior is consistent with the dissociation constants (pKa values) of phosphoric acid, which are approximately 2.14, 7.21, and 12.32 for the stepwise formation of dihydrogen phosphate ($H_2PO_4^-$), hydrogen phosphate (HPO_4^{2-}), and phosphate (PO_4^{3-}) ions, respectively. At pH values of 1–2, the precipitation of REEs is primarily limited due to the presence of undissociated H_3PO_4. As the pH increases, the prevalence of deprotonated phosphoric species alters the equilibrium, favoring the formation of $H_2PO_4^-$ and HPO_4^{2-},leading to the enhanced precipitation of REE phosphates [51]. Thereby, the subsequent neutralization was carried out at 70 °C while the pH was adjusted with 25% ammonium hydroxide. Elevated temperatures reduce the ionization of phosphoric acid and lower the Gibbs energy of the $REEPO_4$ precipitation reaction, thereby enhancing the reaction kinetics and providing more thermodynamically favorable conditions for the precipitation of REEs as phosphates under controlled conditions [44].

According to the ICP-OES elemental analysis of the extracted REEs (Table 5), praseodymium (Pr) and neodymium (Nd) exhibited the highest recovery rates among REEs through the precipitation process, while dysprosium (Dy) and gadolinium (Gd) showed lower efficiencies. This trend corroborated previous findings that the solubility of REEs in phosphoric acid increases with an increase in atomic number, thereby reducing the precipitation efficiency for heavier REEs. Thus, heavy rare earth elements such as Dy tend to have significantly lower recovery rates compared to light rare earth elements like Pr and Nd under similar conditions [44].

X-ray diffraction (XRD) analysis of the treated ERP sample revealed the co-precipitation of REEs with calcium and iron, forming $REPO_4$ and $Ca_3(PO_4)_2$ phases (Figure 5). During the partial neutralization process, the addition of ammonium hydroxide to the nitric–phosphoric acid medium resulted in the formation of ammonium nitrate and ammonium dihydrogen phosphate. As a result, the residual calcium ions also precipitated as $Ca_3(PO_4)_2$ and $Ca(H_2PO_4)_2$. The XRD analysis further confirmed the formation of mixed REE–calcium phosphate phases, as evidenced by the presence of $CaNdCe(PO_4)_3$ phases. The acid leaching of raw ERP at 70 °C facilitated the oxidation of Fe^{2+} to Fe^{3+}. During the partial neutralization step, Fe^{3+} ions precipitated as iron phosphate compounds such as $FeH_2P_2O_7$

and $FePO_4 \cdot 2H_2O$. Given the low solubility product (Ksp) of $FePO_4 \cdot 2H_2O$ (pKsp ≈ 26.4), it readily precipitates even under acidic conditions at low pH levels (pH < 2), contributing to the formation of insoluble precipitates [37]. Even though the temperature was maintained at 70 °C to reduce the solubility of $REEPO_4$ and promote REE precipitation during partial neutralization, this elevated temperature also facilitated the precipitation of $FePO_4 \cdot 2H_2O$, thereby enhancing the co-precipitation of iron. Previous studies have shown that the solubility of $FePO_4 \cdot 2H_2O$ decreases with increasing temperature, which helps stabilize the precipitate [52]. However, the co-precipitation of Ca and Fe under these conditions leads to a substantial reduction in the REE concentration in the leachate. A considerable amount of phosphate is also removed through this process, potentially contributing to a reduction in phosphorus content in the final nitrophosphate fertilizer product. The disappearance of fluorapatite, chlorapatite, and hydroxyapatite peaks in the XRD pattern after leaching indicates the release of anions (F^-, Cl^-, OH^-) into the solution. Depending on the pH and calcium concentration, fluoride may partially precipitate as CaF_2, and hydroxyl as $Ca(OH)_2$ due to the limited solubility in acidic media. The rest of the fluoride likely remains dissolved or evolves as HF under strongly acidic conditions. Chloride ions may remain in the aqueous phase due to their solubility and be removed during subsequent neutralization and washing steps. The absence of these anions in the final fertilizer confirms their effective removal during the process.

Following the partial neutralization, REEs in the precipitate were concentrated via the selective dissolution of REEs by using a mixture of sulfuric and phosphoric acids. The addition of an acid mixture created a highly acidic environment with a low pH, generating a pH gradient between $REPO_4$ and $Ca(H_2PO_4)_2$, thereby enhancing the solubility of $REPO_4$ and $FePO_4 \cdot 2H_2O$ at low-pH conditions. This process was conducted at room temperature., as the solubility of rare earth phosphates in phosphoric acid significantly decreases with increasing temperature [53]. Previous studies have shown that, in addition to $REPO_4$, $Ca_3(PO_4)_2$ and $Ca(H_2PO_4)_2$ can also dissolve in this acidic medium. In the presence of sulfate ions, Ca subsequently precipitates as $CaSO_4$, facilitated by the substitution of HPO_4^{2-} ions with SO_4^{2-} ions in the crystal lattice. The overall ionic equilibrium is driven by the high solubility of REE^{3+} ions in acidic media, contrasted with the low solubility of $CaSO_4$ in the same acidic media under the same conditions [40]. Nearly all REEs were dissolved in the supernatant, indicating minimal incorporation of REEs into calcium sulfate under these specific experimental conditions.

The REEs present in the solution were selectively precipitated by introducing the sodium ion sources, such as NaCl or Na_2SO_4, leading to the formation of $NaREE(SO_4)_2 \cdot xH_2O$. The variation observed in REE recovery efficiencies (ε) is primarily influenced by differences in their ionic characteristics and chemical behavior in solutions. Heavier REEs such as dysprosium (Dy) have smaller ionic radii and higher charge densities, which promote stronger interactions with sulfate ions. As a result, they tend to form stable and less soluble double sulfate salts, such as $NaDy(SO_4)_2 \cdot H_2O$, leading to more efficient precipitation and higher recovery. In contrast, mid-series REEs like gadolinium (Gd) and lighter ones such as praseodymium (Pr) possess larger ionic sizes and lower charge densities. This makes their sulfate complexes more soluble under similar conditions, resulting in comparatively lower recovery efficiencies. These differences in behavior are well-documented in REE precipitation studies and align with established trends in sulfate-based separation systems. In solutions already enriched with sulfate ions (SO_4^{2-}), the introduction of Na^+ shifts the equilibrium toward the formation of these double sulfate phases. REE^{3+} ions have a strong affinity for sulfate ligands due to their comparable ionic radii and high charge density. Despite the presence of chloride ions from NaCl, thermodynamic evidence from previous studies indicates that sulfate ions have a significantly higher tendency to form

more stable complexes with REE^{3+} ions than chloride ions [54]. Consequently, REEs are more likely to precipitate as $NaREE(SO_4)_2 \cdot xH_2O$ than $RECl_3$. Furthermore, the presence of excess SO_4^{2-} ions in the solution induces a common ion effect, significantly reducing the solubility of $NaREE(SO_4)_2 \cdot xH_2O$ and promoting precipitation. The recovered solid product contained 22.2 wt.% REEs from the total weight of the $NaREE(SO_4)_2 \cdot xH_2O$, indicating a successful recovery of REEs. However, it is important to note that the potentially low solubility of $NaREE(SO_4)_2 \cdot xH_2O$ in the acidic medium used for sample preparation for ICP-OES analysis may have contributed to incomplete dissolution, potentially leading to an underestimation of the actual REE recovery.

The integration of REE extraction with nitrophosphate fertilizer production from Eppawala apatite allows for efficient and comprehensive utilization of the raw material, with minimal residual waste. All major constituents of the apatite are transformed into value-added products, highlighting the process's potential for sustainable resource use.

Furthermore, the final fertilizer product was analyzed using SEM-EDX, which revealed no detectable levels of REEs or heavy metals. This indicates that these potentially hazardous elements were effectively separated during the upstream recovery steps and did not carry over into the end product. This is particularly important for agricultural applications.

5. Conclusions

This research demonstrates a unique approach to extracting rare earth elements through the production of nitrophosphate fertilizer using rock phosphate, specifically Sri Lanka's Eppawala apatite rock. The acid leaching process was optimized, and the following optimal leaching parameters were determined: 10 M nitric acid, 2.4 mL/g pulp density, 70 °C leaching temperature, and 120 min of leaching time. Calcium, the major impurity of this process, was effectively removed through a combination of cooling crystallization and selective dissolution of REEs. Furthermore, the partial neutralization process facilitated the formation of a REE phosphate concentrate, resulting in a high REE recovery rate exceeding 90%. The extraction efficiency of individual REEs followed the order Pr > Nd > Ce > Gd > Sm > Y > Dy. Although $REPO_4$ exhibited a high precipitation efficiency, other compounds, such as $Ca_3(PO_4)_2$, $FeH_2P_2O_7$, and $FePO_4.2H_2O$ were also found to co-precipitate with $REPO_4$. The remaining filtrate obtained after the separation of $REPO_4$ during the partial neutralization process was further utilized in the full neutralization process to produce nitrophosphate fertilizer. This not only adds value by utilizing the remaining nutrients but also integrates REE recovery into a fertilizer production pathway, promoting sustainable resource utilization.

A sulfuric–phosphoric acid solution was employed to selectively dissolve REEs from the REE–phosphate phase, achieving an extraction efficiency of over 99%, while calcium remained in the solid form as $CaSO_4$. At this stage, REEs have been effectively recovered through the nitrophosphate fertilizer production process, showing its viability as a dual-purpose method for both fertilizer generation and REE extraction from apatite-based resources. To improve both the efficiency and purity of REE recovery via the sodium REE double sulfate route, further optimization of the process steps is required. Additionally, the selective recovery of individual REEs can be enhanced through advanced solvent extraction techniques.

The ERP-based nitrophosphate fertilizer product exhibited desirable agronomic characteristics, such as a high nitrogen content of 18.2%, high phosphorous content of 13.9% as P_2O_5, low moisture content of 0.6%, and free acid level of 0.1%. These characteristics suggest that nitric acid digestion of ERP can yield a nutrient-rich, physically stable fertilizer suitable for large-scale application and for phosphorus-deficient and nitrogen-deficient agricultural systems.

In summary, this study introduces a resource-efficient route to simultaneously valorize apatite deposits for fertilizer production and REE recovery, supporting the principles of a circular economy. Future studies should focus on field validation and advanced separation technologies for enhancing individual REE selectivity.

Supplementary Materials: The following supporting information can be downloaded at https://www.mdpi.com/article/10.3390/su17146353/s1: Table S1. Digestion efficiency and P_2O_5 decomposition at different nitric acid concentrations in acid leaching of ERP; Table S2. REE leaching efficiency % with different nitric acid concentrations in acid leaching of ERP; Table S3. Digestion efficiency and P_2O_5 decomposition at different leaching temperatures in acid leaching of ERP; Table S4. REE leaching efficiency % with different acidolysis temperatures in acid leaching of ERP; Table S5. Digestion efficiency and P_2O_5 decomposition at different leaching times in acid leaching of ERP; Table S6. REE leaching efficiency % with different acidolysis times in acid leaching of ERP; Table S7. Digestion efficiency and P_2O_5 decomposition at different leaching times in acid leaching of ERP; Table S8. REE leaching efficiency % with different pulp densities in acid leaching of ERP; Figure S1. Synthesized sample of $Ca(NO_3)_2{\cdot}4H_2O$(S); Figure S2. Synthesized sample of $REEPO_4$(S); Figure S3. Synthesized sample of $CaSO_4$(S); Figure S4. Synthesized sample of $NaREE(SO_4)_2{\cdot}xH_2O$(S).

Author Contributions: Conceptualization, P.W.S. and D.B.H.I.B.; Methodology, P.W.S. and D.B.H.I.B.; Validation, D.B.H.I.B., A.P. and K.D.A.D.; Formal Analysis, D.B.H.I.B. and K.D.A.D.; Investigation, D.B.H.I.B.; Resources, P.W.S.; Data Curation, D.B.H.I.B., K.D.A.D. and A.P.; Writing—Original Draft Preparation, D.B.H.I.B.; Writing—Review and Editing, P.W.S.; Visualization, D.B.H.I.B.; Supervision, P.W.S.; Project Administration, P.W.S.; Funding Acquisition, P.W.S. All authors have read and agreed to the published version of the manuscript.

Funding: This research was supported by the Science and Technology Human Resource Development Project, Ministry of Higher Education, Sri Lanka, funded by the Asian Development Bank (Grant No. CRG/R2/KE6).

Institutional Review Board Statement: Not applicable.

Informed Consent Statement: Not applicable.

Data Availability Statement: Data is contained within the article or Supplementary Materials.

Acknowledgments: The authors thankfully acknowledge the Faculty of Computing and Technology, University of Kelaniya, Sri Lanka, for facilitating the work and the analytical support provided by the Geological Survey and Mining Bureau, Industrial Technology Institute, and Sri Lanka Institute of Nanotechnology.

Conflicts of Interest: The authors declare no conflicts of interest.

References

1. Drobniak, A.; Mastalerz, M. Rare Earth Elements: A brief overview. *Indiana J. Earth Sci.* **2022**, *4*, 1–7. [CrossRef]
2. Suli, L.M.; Ibrahim, W.H.W.; Aziz, B.A.; Deraman, M.R.; Ismail, N.A. A Review of Rare Earth Mineral Processing Technology. *Chem. Eng. Res. Bull.* **2017**, *19*, 20. [CrossRef]
3. Du, X.; Graedel, T.E. Global in-use stocks of the rare earth elements: A first estimate. *Environ. Sci. Technol.* **2011**, *45*, 4096–4101. [CrossRef]
4. Balaram, V. Rare earth elements: A review of applications, occurrence, exploration, analysis, recycling, and environmental impact. *Geosci. Front.* **2019**, *10*, 1285–1303. [CrossRef]
5. Rupasinghe, M.S.; Dissanayake, C.B. The rare-earth element abundance in the sedimentary gem deposits of Sri Lanka. *Lithos* **1984**, *17*, 329–342. [CrossRef]
6. Lin, P.; Yang, X.; Werner, J.M.; Honaker, R.Q. Application of Eh-pH Diagrams on Acid Leaching Systems for the Recovery of REEs from Bastnaesite, Monazite and Xenotime. *Metals* **2021**, *11*, 734. [CrossRef]
7. Vinoj, P.K.L.; Kapilarathna, M.W.C.S.; Samarakoon, S.M.P.S.; Dushyantha, N.P. Investigation of Rare Earth Element Potential in Granitic Rocks of Sri Lanka Special Reference to Thonigala Granite. In Proceedings of the International Symposium on Earth Resources Management & Environment, Jakarta, Indonesia, 25–26 September 2021; pp. 128–134.

8. Dostal, J. Rare earth element deposits of alkaline igneous rocks. *Resources* **2017**, *6*, 34. [CrossRef]
9. Dissanayake, C.B.; Chandrajith, R.; Tobschall, H.J. The geology, mineralogy and rare element geochemistry of the gem deposits of Sri Lanka. *Bull. Geol. Soc. Finl.* **2000**, *72*, 5–20. [CrossRef]
10. Toama, H.Z. World Phosphate Industry. *Iraqi Bull. Geol. Min. Spec. Issue* **2017**, *7*, 5–23.
11. Guelfi, D.; Nunes, A.P.P.; Sarkis, L.F.; Oliveira, D.P. Innovative Phosphate Fertilizer Technologies to Improve Phosphorus Use Efficiency in Agriculture. *Sustainability* **2022**, *14*, 4266. [CrossRef]
12. Khan, M.; Ahmad, S.; Sharif, M.; Billah, M.; Aslam, M. Formulation of single super phosphate fertilizer from rock phosphate of Hazara, Pakistan. *Soil Environ.* **2012**, *31*, 96–99.
13. Reijnders, L. Phosphorus resources, their depletion and conservation, a review. *Resour. conserv. recycl.* **2014**, *93*, 32–49. [CrossRef]
14. Hughes, J.M.; Rakovan, J. The crystal structure of apatite, $Ca_5(PO_4)_3(F,OH,Cl)$. *Phosphates Geochem. Geobiol. Mater. Importance* **2019**, *48*, 1–12. [CrossRef]
15. Cheremisina, O.; Sergeev, V.V.; Fedorov, A. Rare Earth Metal Extraction from Apatite Ores. *Metallurgist* **2019**, *63*, 300–307. [CrossRef]
16. Gamage, S. Determination of Rare Earth Element Contents in the Pulmoddai-Based Monazite. *Int. J. Adv. Res.* **2018**, *6*, 1229–1236. [CrossRef]
17. Manthilake, M.A.G.M.; Sawada, Y.; Sakai, S. Genesis and evolution of Eppawala carbonatites, Sri Lanka. *J. Asian Earth Sci.* **2008**, *32*, 66–75. [CrossRef]
18. Batapola, N.M.; Dushyantha, N.P.; Premasiri, H.M.R.; Abeysinghe, A.M.K.B.; Rohitha, L.P.S.; Ratnayake, N.P.; Dissanayake, D.M.D.O.K.; Ilankoon, I.M.S.K.; Dharmaratne, P.G.R. A comparison of global rare earth element (REE) resources and their mineralogy with REE prospects in Sri Lanka. *J. Asian Earth Sci.* **2020**, *200*, 104475. [CrossRef]
19. Dushyantha, N.; Batapola, N.M.; Ratnayake, N.P. Leaching Potential of Rare Earth Elements (REES) from Eppawala Phosphate Deposit, Sri Lanka for Sustainable Critical Metals Recovery. In Proceedings of the 39th Technical Session of Geological Society of Sri Lanka (GSSL), Kandy, Sri Lanka, 24 February 2023; p. 6.
20. Ribeiro, G.P.; Dantas, S.C.; Ribeiro, E.J.; Hori, C.E. Production of Single Superphosphates Using Igneous Phosphate Rocks with High Iron Oxide Concentrations. *Ind. Eng. Chem. Res.* **2023**, *62*, 12963–12973. [CrossRef]
21. Udawatte, C.P.; Panagoda, P.V.A.; Wickramasinghe, W.M.A.D.B.; Wijewardena, J.D.H.; Sirisena, D.N.; Emitiyagoda, S.; Bandara, H.R.U.D. Use of single superphosphate fertiliser produced using eppawala rock phosphate as a source of phosphorous for rice cultivation. *J. Natl. Sci. Found. Sri Lanka* **2020**, *48*, 131–142. [CrossRef]
22. Idi, A.A.B.; Ousmane, M.I.C.; Sahirou, B.M.; Manzola, A.S. Manufacture of simple superphosphate from Tahoua rock phosphate. *World J. Adv. Res. Rev.* **2023**, *18*, 1139–1148. [CrossRef]
23. Nicola Doebelin, R.K. Profex: A graphical user interface for the Rietveld refinement program BGMN. *J. Appl. Crystallogr.* **2015**, *48*, 1573–1580. [CrossRef]
24. Sri Lanka Standards Institution. Methods of Test for Fertilizers and Soil Conditioners Part 2: Determination of Moisture and Ash (First Revision). 2023. Available online: https://slsi.lk/web/wp-content/uploads/2023/04/DSLS-645-2.pdf (accessed on 22 April 2025).
25. Vindiola, A.G., Jr. Laboratory Safety. In *Official Methods of Analysis of AOAC International*, Latimer, G.W., Ed.; 22nd ed.; AOAC Publications: New York, NY, USA, 2023.
26. Sri Lanka Standards Institution (SLS). Methods of Test for Fertilizers and Soil Conditioners Part 1: Determination of Nitrogen (Second Revision). 2023. Available online: https://slsi.lk/web/wp-content/uploads/2023/04/SLS-645-1.pdf (accessed on 20 April 2025).
27. Sri Lanka Standards Institution (SLS). *Methods of Test for Fertilizers and Soil Con Ditioners Part 5: Determination of Phosphorous*; Sri Lanka Standards Institution (SLS): Colombo, Sri Lanka, 1985.
28. Sri Lanka Standards Institution (SLS). *Triple Super-Phosphate (Fertilizer Grade)*; Sri Lanka Standards Institution (SLS): Colombo, Sri Lanka, 2014.
29. Zuo, R.F.; Du, G.X.; Yang, W.G.; Liao, L.B.; Li, Z. Mineralogical and chemical characteristics of a powder and purified quartz from Yunnan Province. *Open Geosci.* **2016**, *8*, 606–611. [CrossRef]
30. García-Tuñón, E.; Couceiro, R.; Franco, J.; Saiz, E.; Guitián, F. Synthesis and characterisation of large chlorapatite single-crystals with controlled morphology and surface roughness. *J. Mater. Sci. Mater. Med.* **2012**, *23*, 2471–2482. [CrossRef] [PubMed]
31. Kostov-Kytin, V.V.; Dyulgerova, E.; Ilieva, R.; Petkova, V. Powder X-ray diffraction studies of hydroxyapatite and β-TCP mixtures processed by high energy dry milling. *Ceram. Int.* **2018**, *44*, 8664–8671. [CrossRef]
32. Loy, C.W.; Matori, K.A.; Zainuddin, N.; Whitten, A.E.; Rehm, C.; de Campo, L.; Sokolova, A.; Schmid, S. Crystallographic characterization of fluorapatite glass-ceramics synthesized from industrial waste. *Powder Diffr.* **2017**, *32*, S61–S65. [CrossRef]
33. Dahanayake, K.; Subasinghe, S.M.N.D. Mineralogical, chemical and solubility variations in the Eppawala phosphate deposit of Sri Lanka—A case for selective mining for fertilizers. *Fertil. Res.* **1991**, *28*, 233–238. [CrossRef]

34. Liu, Y.; Li, Z.; You, Y.; Zheng, X.; Wen, J. Synthesis of different structured FePO4 for the enhanced conversion of methyl cellulose to 5-hydroxymethylfurfural. *RSC Adv.* **2017**, *7*, 51281–51289. [CrossRef]
35. Pralong, V.; Baies, R.; Calgnaert, V.; Raveau, B. Structure and physical properties of new iron hydrogenophosphates $K_2Fe(HP_2O_7)(H_2PO_4)_2$, $LiH_3Fe_2(P_2O_7)_2$, and $FeH_2P_2O_7$. *Inorg. Chem.* **2009**, *48*, 6835–6844. [CrossRef]
36. Ardanova, L.I.; Get'Man, E.I.; Loboda, S.N.; Prisedsky, V.V.; Tkachenko, T.V.; Marchenko, V.I.; Antonovich, V.P.; Chivireva, N.A.; Chebishev, K.A.; Lyashenko, A.S. Isomorphous substitutions of rare earth elements for calcium in synthetic hydroxyapatites. *Inorg. Chem.* **2010**, *49*, 10687–10693. [CrossRef]
37. Alemrajabi, M. Recovery of Rare Earth Elements from an Apatite Concentrate. Ph.D. Thesis, KTH Royal Institute of Technology, Stockholm, Sweden, 2018. Available online: https://www.diva-portal.org/smash/get/diva2:1263554/FULLTEXT01.pdf (accessed on 15 January 2024).
38. Roy, R.N. Use of Phosphate Rocks for Sustainable Agriculture. Zapata, F., Ed.; FAO Land and Water Development Division and the International Atomic Energy Agency: Rome, Italy, 2004.
39. Kim, R.; Cho, H.; Han, K.N.; Kim, K.; Mun, M. Optimization of Acid Leaching of Rare-Earth Elements from Mongolian Apatite-Based Ore. *Minerals* **2016**, *6*, 63. [CrossRef]
40. Alemrajabi, M.; Rasmuson, Å.C.; Korkmaz, K.; Forsberg, K. Upgrading of a rare earth phosphate concentrate within the nitrophosphate process. *J. Clean. Prod.* **2018**, *198*, 551–563. [CrossRef]
41. Stone, K.; Bandara, A.M.T.S.; Senanayake, G.; Jayasekera, S. Processing of rare earth phosphate concentrates: A comparative study of pre- leaching with perchloric, hydrochloric, nitric and phosphoric acids and deportment of minor/major elements. *Hydrometallurgy* **2016**, *163*, 137–147. [CrossRef]
42. Meor, Y.M.S. Rate of rare earths leaching in HCI, H_2SO_4 AND HNO_3. *Adv. Mater. Res.* **2013**, *795*, 1–4. [CrossRef]
43. Premasiri, H.M.R. Leaching Potential of Rare Earth Elements (REES) from Eppawala Phosphate Deposit, Sri Lanka for Sustainable Critical Metals Recovery. In Proceedings of the Geological Society of Sri Lanka (GSSL), Kandy, Sri Lanka, 24 February 2023; pp. 1–2.
44. Wu, S.; Zhao, L.; Wang, L.; Huang, X.; Dong, J.; Feng, Z.; Cui, D.; Zhang, L. feng Dissolution behaviors of rare earth elements in phosphoric acid solutions. *Trans. Nonferrous Met. Soc. China (Engl. Ed.)* **2018**, *28*, 2375–2382. [CrossRef]
45. Li, H.; Guo, F.; Zhang, Z.; Li, D.; Wang, Z. A new hydrometallurgical process for extracting rare earths from apatite using solvent extraction with P_{350}. *J. Alloys Compd.* **2006**, *412*, 995–998. [CrossRef]
46. Habashi, F. The Recovery of the Lanthanides from Phosphate Rock. *J. Chem. Technol. Biotechnol.* **1985**, *4*, 5–14. [CrossRef]
47. Liu, X.; Byrne, R.H. Rare earth and yttrium phosphate solubilities in aqueous solution. *Geochim. Cosmochim. Acta* **1997**, *61*, 1625–1633. [CrossRef]
48. Sigtryggsson, C.; Hamnér, K.; Kirchmann, H. Laboratory studies on dissolution of nitrogen fertilizers by humidity and precipitation. *Agric. Environ. Lett.* **2020**, *5*, e20016. [CrossRef]
49. P, D. CRC Handbook of Chemistry and Physics: Editor-in-chief D.R. Lide; CRC Press, Boca Raton, FL, USA, 71st edn, 1990–1991, pp. 2324, price $117.00 (USA $99.50). *J. Mol. Struct.* **1992**, *268*, 320. [CrossRef]
50. Beaumont, A.B.; Mooney, R.A. Hygroscopicity and Cakiness of Fertilizer Materials. *Ind. Eng. Chem.* **1925**, *17*, 635–636. [CrossRef]
51. Han, K.N. Characteristics of precipitation of rare earth elements with various precipitants. *Minerals* **2020**, *10*, 178. [CrossRef]
52. Zhang, T.; Lu, Y.; Luo, G. Effects of temperature and phosphoric acid addition on the solubility of iron phosphate dihydrate in aqueous solutions. *Chin. J. Chem. Eng.* **2017**, *25*, 211–215. [CrossRef]
53. Cetiner, Z.S.; Wood, S.A.; Gammons, C.H. The aqueous geochemistry of the rare earth elements. Part XIV. The solubility of rare earth element phosphates from 23 to 150 °C. *Chem. Geol.* **2005**, *217*, 147–169. [CrossRef]
54. Cui, H.; Zhong, R.; Xie, Y.; Yuan, X.; Liu, W.; Brugger, J.; Yu, C. Forming sulfate-and REE-rich fluids in the presence of quartz. *Geology* **2020**, *48*, 145–148. [CrossRef]